Ionic liquid-assisted hydrothermal synthesis of β-$Ni(OH)_2$ nanoflakes and the application of NiO in lithium-ion battery

XIAODI LIU*, HAO CHEN, LIQUN YE, WENHUI SHANG
College of Chemistry and Pharmaceutical Engineering, Nanyang Normal University, Nanyang 473061, China

β-$Ni(OH)_2$ nanoflakes have been synthesized through a hydrothermal route with the assistance of ionic liquid 1-butyl-3-methylimidazolium bromide ([Bmim]Br). The β-$Ni(OH)_2$ nanoflakes are about 100 nm in edge length and 50 nm in thickness. More importantly, [Bmim]Br plays a critical role for the formation of flake-like β-$Ni(OH)_2$ by adsorbing on the OH^- ions coordinated with Ni^{2+} ions on (001) planes. The β-$Ni(OH)_2$ nanoflakes can be converted into NiO *via* a thermal decomposition process and the obtained NiO nanostructures exhibit a capacity of 1157.6 $mAhg^{-1}$ at 0.1 C when employed as anode materials in lithium-ion batteries.

(Received August 2, 2013; accepted January 22, 2014)

Keywords: β-$Ni(OH)_2$, Nanoflakes, Ionic liquid, Hydrothermal method

1. Introduction

It is known that the shape, dimension, and size of nanomaterials have great influence on their physical and chemical properties and related applications; thereafter, morphology-control of nanomaterials has become an important goal of materials chemistry [1]. More recently, a variety of nanomaterials with controlled morphologies have been fabricated; nevertheless, these nanomaterials generally are prepared by using various organic solvents or templates [2-5]. Ionic liquids (ILs), consisting of predominantly ionic species, have attracted tremendous attention for their unique physico-chemical properties. ILs are wildly used as "green" solvents in many fields; furthermore, the advantages of ILs in inorganic synthesis have been gradually realized and several nanomaterials with novel morphologies have been synthesized [6-8]. However, the exploration of ILs for the synthesis of nanomaterials is still in its infancy, and the application of ILs in inorganic synthesis should be intensively investigated.

$Ni(OH)_2$, as one of the most important transition metal hydroxides, has been used as active material of the positive electrode in alkaline rechargeable Ni-based battery [9,10]. Additionally, $Ni(OH)_2$ can be converted into NiO, which has been exploited as a lithium-ion battery material for the higher electrochemical capacity than that of the commercial graphite anode material [11]. It has been reported that the morphologies of $Ni(OH)_2$ and NiO nanostructures have great influence on their electrochemical utilization; therefore, $Ni(OH)_2$ and NiO nanomaterials with various shapes have been fabricated [12-14]. Most particularly, 2D flake-like nanostructures are of great importance from both fundamental and applied perspectives [15]. Nevertheless, there are only a few reports on the synthesis of $Ni(OH)_2$/NiO nanoflakes and strong alkaline medium are commonly used [16-19]. Thus, in spite of these successes, it is still a challenge to explore facile, effective, and environmentally benign routes for the fabrication of $Ni(OH)_2$ and NiO nanoflakes with uniform morphology and improved properties.

Herein, β-$Ni(OH)_2$ nanoflakes have been prepared *via* a hydrothermal method with the assistance of IL 1-butyl-3-methylimidazolium bromide ([Bmim]Br). The synthetic system, which just uses [Bmim]Br-water as solvent, is very simple; moreover, β-$Ni(OH)_2$ nanoflakes can be prepared at relatively low OH^- concentration. The as-formed β-$Ni(OH)_2$ nanoflakes have smooth surfaces and relatively symmetrical hexagonal shapes. β-$Ni(OH)_2$ nanoflakes can be easily converted into NiO by a thermal decomposition process; moreover, NiO nanostructures have been investigated as anode materials for lithium-ion battery.

2. Experimental sections

Chemicals: All chemicals used in the experiment were of analytical grade and used without purification. IL 1-*n*-butyl-3-methylimidazolium bromide ([Bmim]Br) was prepared according to the literature [20].

Synthesis of *β*-nickel hydroxide and nickel oxide nanoflakes: In a typical experiment, $NiSO_4 \cdot 6H_2O$ (0.039 g) and [Bmim]Br (1.5 g) were dissolved in 7.5 mL deionized water to form a clear solution and aged 5 min; then 7.5 mL NaOH solution (0.02 $mol \cdot L^{-1}$) were added into the solution; in the end, the solution was stirred 20 min at room temperature and transferred into a stainless steel Teflon-lined autoclave (20 mL). The autoclave was sealed and maintained at 120 °C for 12 h. After the autoclave was cooled to room temperature, the precipitate was collected by centrifugation, washed with deionized water and anhydrous ethanol, and then dried at 50 °C for 5 h. Finally light green powders were obtained. NiO nanostructures (black powders) could be gained by thermal decomposition of $Ni(OH)_2$ nanoflakes at 400 °C for 2 h in muffle furnace in air condition.

Characterization and instruments: The phase compositions and purities of the samples were examined by X-ray powder diffraction (XRD) on a Rigaku D/max 2500V/PC X-ray powder diffractometer with Cu Kα radiation (λ = 1.54056). The sizes and morphologies of the products were characterized with a FEI-Quanta-200 scanning electron microscope (SEM). The transmission electron microscope (TEM) was taken with a Hitachi H-7650 transmission electron microscope.

Electrochemical measurements: The Li storage performance was investigated in Li test cells for the NiO sample. The anode electrodes were made of 75 wt% NiO nanoflakes, 15 wt% acetylene black, and 10 wt% polytetrafluoroethylene (PTME) in ethanol. The electrodes were dried at 120 °C for 10 h in air. Lithium metal was used as the counter electrode. The electrolyte was composed of a 1 M $LiPF_6$ dissolved in ethylene carbonate (EC)-diethyl carbonate (DEC) (50/50 vol.%). For cycling experiments, the cells were measured at different current densities (0.1, 0.2, 1, and 2 C) within a voltage range of 0.01-3.0 V with a Land CT2001 battery tester at 25 °C.

3. Results and discussion

The crystal structure of the obtained $Ni(OH)_2$ were characterized by XRD and the result is shown in Fig. 1a. All diffraction peaks can be indexed to hexagonal *β*-$Ni(OH)_2$ with the lattice parameters of $a = b = 3.126$ Å and $c = 4.605$ Å, which is in good agreement with the literature values (JCPDS No. 14-0117). No peaks due to *α*-$Ni(OH)_2$ are observed. Compared to the standard XRD pattern of *β*-$Ni(OH)_2$, the (001) reflection peak is remarkably enhanced and appears as the strongest peak, indicating that the *β*-$Ni(OH)_2$ is oriented-growth and the [001] planes are predominant in the *β*-$Ni(OH)_2$ [21]. The sizes and morphologies of the *β*-$Ni(OH)_2$ are investigated by SEM and TEM. SEM image (Fig. 1b) shows that the products are almost entirely nanoflakes with smooth surfaces and hexagonal shapes. The high-magnified SEM image (inset of Fig. 1b) indicates that these nanoflakes are about 100 nm in edge length and 50 nm in thickness. The TEM result, Fig. 1c, displays that the sizes of the products are consistent with the results observed in SEM images and the *β*-$Ni(OH)_2$ nanoflakes are well dispersed with good monodispersity, which is in favour of some potential applications such as Ni/MH battery [22].

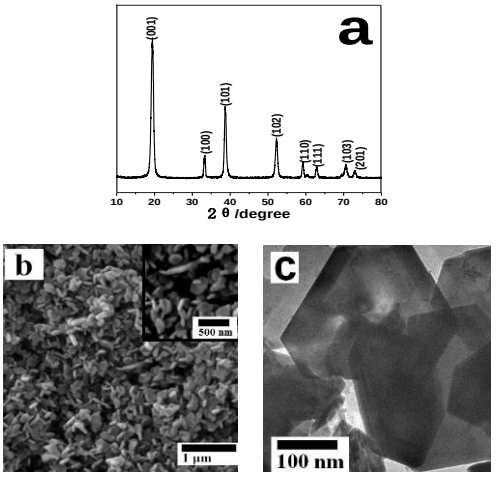

Fig. 1. (a) XRD pattern, (b) SEM image, and (c) TEM image of the obtained β-Ni(OH)$_2$ nanoflakes, the inset of (b) is the high-magnified SEM image.

Generally, the intrinsic shape of nanocrystals is dominated by the crystalline structure of initial seeds and the final shape is also governed by the subsequent growth stage through delicate control of external factors (i.e., capping molecules and reaction temperature) [6]. For anisotropic unit cell structure, the selective anisotropic growth along the crystallographic reaction directions is facilitated, which results in special shapes (e.g., rods, plates) [23]. *β*-$Ni(OH)_2$ has a hexagonal cell based on the P-3m1(164) space group and adopts a CdI_2-type layer structure. As depicted in Fig. 2a, Ni^{2+} ions are octahedrally coordinated by six OH^- ions, and the stacking of the Ni^{2+} layers is hexagonal, with alternate layers directly above and below each other. Strong covalent ionic bonds hold the atoms within the layers [24]. It is known that the crystalline facets tend to develop on the low-index planes to minimize the surface energy during the growth process, so it is reasonably speculated that the intrinsic anisotropic structure of *β*-$Ni(OH)_2$ can result in the rate of crystal growth along the top-bottom crystalline planes becoming greater than that along *c*-axis, which can dominate the shape of the primary *β*-$Ni(OH)_2$ particles (e.g., platelet seed) [15, 25]. In fact, when the concentration of OH^- in the solution is high, the (001) planes possess higher hydroxyl concentration than (100) and (010) planes, which could result in high repulsive effect, and accordingly the crystals tend to grow along (001) plane [26].

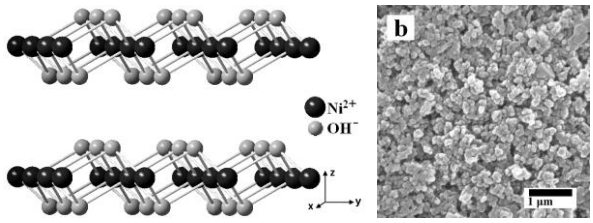

Fig. 2. (a) Schematic illustration of the crystal structure of β-Ni(OH)$_2$; (b) SEM image of the β-Ni(OH)$_2$ synthesized with no [Bmim]Br and keeping other reaction parameters unchanged.

In our experiment, the ratio of Ni^{2+}/OH^- in the reactants is just 1:1, which is not benefit for the formation of nanoflakes. Fortunately, we have found that [Bmim]Br has effect on the morphology of β-Ni(OH)$_2$ nanoflakes. The cations of IL ([Bmim]$^+$) are prone to adsorb on the OH^- coordinated with Ni^{2+} on (001) planes driven by electrostatic force and owing to steric hindrance, thus the growth of the β-Ni(OH)$_2$ along the [001] direction is suppressed and β-Ni(OH)$_2$ preferentially grow along (001) plane to form flake-like products, consisting with the XRD result (Fig. 1a) [27]. In order to further substantiate the effect of [Bmim]Br, we have carried out a control experiment, in which no [Bmim]Br is added and other parameters are unchanged. Finally, as shown in Fig. 2b, β-Ni(OH)$_2$ nanocrystals with irregular morphology and a few β-Ni(OH)$_2$ microcrystals coexist in the products.

According to the above detailed discussion, the possible growth mechanism of β-Ni(OH)$_2$ nanoflakes has been given and a schematic illustration is presented in Fig. 3. Firstly, lots of β-Ni(OH)$_2$ nanocrystals can be easily formed in the presence of [Bmim]Br owing to its high ionic conductivity and lower surface tension compared with water [28]. Then, [Bmim]Br can reduce the preferential growth of β-Ni(OH)$_2$ crystal nuclei in certain direction. In addition, the using of [Bmim]Br can increase of the nuclear rate; therefore, the sample is in the growth process for the most of the reaction time (Ostwald ripening) [14]. Finally, β-Ni(OH)$_2$ nanocrystals grow into nanoflakes in the growth process.

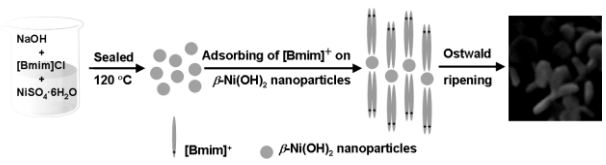

Fig. 3. Schematic illustration of the possible growth mechanism of the β-Ni(OH)$_2$ nanoflakes.

The nickel hydroxyl can easily be converted into nickel oxide upon heat treatment. Fig. 4a shows the XRD pattern of the obtained NiO nanomaterials. All the diffraction peaks match well with the cubic NiO with the lattice parameters of $a = b = c = 4.179$ Å (JCPDS No. 71-1179). No peaks due to β-Ni(OH)$_2$ are observed by XRD, which indicates that β-Ni(OH)$_2$ is completely transformed to NiO. The as-formed NiO nanostructures also exhibits flake-like morphology when the β-Ni(OH)$_2$ nanoflakes were annealed at 400 °C for 2 h, which is similar to the literatures [27, 29]. Fig. 4b displays the voltage-capacity curves of the NiO nanostructures in the first discharge-charge cycle at different current densities (0.1, 0.2, 1, and 2 C). It can be seen that a high discharge capacity of 1157.6 mAhg^{-1} can be obtained in the first discharge process at a low current density of 0.1 C (curve A). In addition, in the charge process, the capacity of the electrode is 709 mAhg^{-1}, which is lower that that of the corresponding discharge process. The ratio of the charge retention is about 61.2%. In addition, during the first discharge, the discharge capacity for NiO nanostructures is 1116, 1021, and 862 mAhg^{-1} at 0.2, 1, and 2 C, respectively. The result suggests that the nanoflakes are helpful for improving the electrochemical performance of nickel oxide.

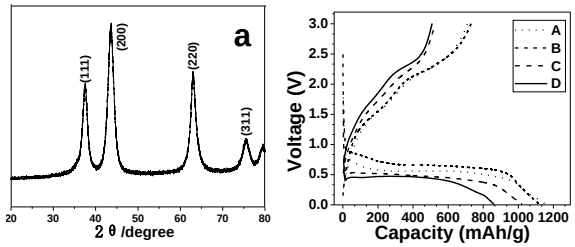

Fig. 4. (a) XRD pattern of the NiO nanostructures, (b) First discharge-charge curves of the NiO nanostructures at different current densities (a: 0.1 C, b: 0.2 C, c: 1 C, d: 2 C).

4. Conclusion

In summary, β-Ni(OH)$_2$ nanoflakes have been synthesized *via* a ionic liquid-assisted hydrothermal method and the application of NiO nanostructures in lithium-ion battery has been researched. The significance of this work is fourfold. First, this method provides a facile, effective, and environmentally benign route to the nanosized β-Ni(OH)$_2$ flakes. Second, [Bmim]Br, as "green" organic solvent with high ionic conduction and low surface tension, makes the nucleation easily and facilitates the growth of flake-like β-Ni(OH)$_2$. Three, the as-formed NiO nanostructures shows a high discharge capacity of 1157.6 mAhg^{-1} at 0.1 C, which have promising applications as lithium-ion battery anodes. Four, we expect that this method can be used to prepare other metal hydroxides with special morphologies and further studies are underway to broaden its applicability.

Acknowledgements

This work was supported by The Joint Fund for Fostering Talents of National Science Foundation of China and Henan Province (No. U1304506), Natural Science Foundation of Henan Department of Education (No. 13A150813), National Training Programs of Innovation for Undergraduates (No. 201310481063).

References

[1] K. Shin, H. J. Kin, J. M. Choi, Y. M. Choi, M. S. Song, J. H. Park, Chem. Commun. **49**, 2326 (2013).
[2] G. Tian, Z. Gu, L. Zhou, W. Yin, X. Liu, L. Yan, S. Jin, W. Ren, G. Xing, S. Li, Y. Zhao, Adv. Mater. **24**, 1226 (2012).
[3] R. Liu, D. Tu, Y. Liu, H. Zhu, R. Li, W. Zheng, E. Ma, X. Chen, Nanoscale **4**, 4485, (2012).
[4] T. K. Sau, C. J. Murphy, Langmuir **21**, 2923 (2005).
[5] L. Wang, C. Xu, X. Zhang, T. Ying, Chem. Lett. **26**, 642 (2007).
[6] X. D. Liu, G. Guo, K. Y. Bao, B. Y. Liang, Cryst. Res. Technol. **46**, 205 (2011).
[7] X. D. Liu, X. C. Duan, P. Peng, W. J. Zheng, Nanoscale **3**, 5090 (2011).
[8] T. Nakashima, N. Kimizuka, J .Am. Chem. Soc. **125**, 6386 (2003).
[9] H. M. French, M. J. Henerson, A. R. Hillman, E. Vieil, J. Electroanal. Chem. **500**, 192 (2001).
[10] J. Chen, D. H. Bradhurst, S. X. Dou, H. K. Liu, J. Electrochem. Soc. **146**, 3606 (1999).
[11] X. H. Huang, J. P. Tu, C. Q. Zhang, J. Y. Xiang, Electrochem. Commun. **9**, 1180 (2007).
[12] L. Zhuo M. J. Ge. L. Cao, B. Tang, Cryst. Growth Des. **9**, 1 (2009).
[13] L. P. Zhu, G. H. Liao, Y. Yang, H. M .Xiao, J. F. Wang, S. Y. Fu, Nanoscale Res. Lett. **4**, 550 (2009).
[14] Y. Wang, Q. Zhu, H. Zhang, Chem. Commun. 5231, (2005).
[15] M. Osada, Y. Ebina, K. Takada, T. Sasaki, Adv. Mater. **18**, 295 (2006).
[16] Y. Qi, H. Qi, J. Li, C. Lu, J. Cryst. Growth **310**, 4221 (2008).
[17] L. Dong, Y. Chu, W. Sun, Chem. Eur. J. **14**, 5064 (2008).
[18] H. Jiang, T. Zhao, C. Li, J. Ma, J. Mater. Chem. **21**, 3818 (2011).
[19] D. Chen, L. Gao, Chem. Phys. Lett. **405**, 159 (2005).
[20] P. N. Tshibangu, S. N. Ndwandwe, E. D. Dikio, Int. J. Electrochem. Sci. **6**, 2201 (2011).
[21] S. Zhang, H. C. Zeng, Chem. Mater. **21,** 871 (2009).
[22] I. B. Malham, P. Letellier, M. Turmine, J. Phys. Chem. B **110**, 14212 (2006).
[23] C. Li, J. Yang, P. Yang, X. Zhang, H. Lian, J. Lin, Cryst. Growth Des. **8,** 923 (2008).
[24] J. Ma, J. Yang, L. Jiao, Y. Mao, T. Wang, X. Duan, J. Lian, W. Zheng, Cryst Eng Comm **14**, 453 (2012).
[25] W. Lu, Y. Ding, Y. Chen, Z. L. Wang, J. Fang, J. Am. Chem. Soc. **127**, 10112 (2005).
[26] J. T. Sampanthar, H. C. Zeng, J. Am. Chem. Soc. **124**, 6668 (2002).
[27] S. H. Jung, E. Oh, K. H. Lee, Y. Yang, C. G. Park, W. Park, S. H. Jeong, Cryst. Growth Des. **8**, 265 (2008).
[28] X. D. Liu, J. M. Ma, P. Peng, W. J. Zheng, Mater. Sci. Eng. B **150**, 89 (2008).
[29] C. Tang, G. Li, L. Li, Chem. Lett. **37**, 1138 (2008).

*Corresponding author: liuxiaodiny@126.com